

---

# A Practical Approach for Exploring Granger Connectivity in High-Dimensional Networks of Time Series

---

**Sipan Aslan & Hernando Ombao**  
Statistics Program @KAUST  
King Abdullah University of Science and Technology  
Thuwal, KSA, 29355-6900  
sipan.aslan@kaust.edu.sa  
hernando.ombao@kaust.edu.sa

## Abstract

This paper presents a novel method for discovering effective connectivity between specified pairs of nodes in a high-dimensional network of time series. To accurately perform Granger causality analysis from the first node to the second node, it is essential to eliminate the influence of all other nodes within the network. The approach proposed is to create a low-dimensional representation of all other nodes in the network using frequency-domain-based dynamic principal component analysis (spectral DPCA). The resulting scores are subsequently removed from the first and second nodes of interest, thus eliminating the confounding effect of other nodes within the high-dimensional network. To conduct hypothesis testing on Granger causality, we propose a permutation-based causality test. This test enhances the accuracy of our findings when the error structures are non-Gaussian. The approach has been validated in extensive simulation studies, which demonstrate the efficacy of the methodology as a tool for causality analysis in complex time series networks. The proposed methodology has also been demonstrated to be both expedient and viable on real datasets, with particular success observed on multichannel EEG networks.

## 1 Introduction

Identifying Granger-causal connections between nodes in high-dimensional networks in neuroscience and network science has significant outcomes. This is particularly relevant when analyzing EEG/fMRI data, where the attention is on a few channels/regions of interest within an extensive network of interacting nodes (Friston, 2011; Friston et al., 2013; Yang et al., 2016; Tu et al., 2019). Conventional Granger causality (GC) is the standard approach to infer causal relationships in high-dimensional EEG networks. However, they are subject to substantial limitations due to the impact of extraneous channels on the Channels of Interest (COI). Accordingly, there is a need for an effectual and parsimonious method to isolate and accurately evaluate the COI's causal interactions, especially in the presence of multiple channels. The prevailing approaches to causality analysis in high-dimensional networks typically depend on F-tests for Granger causality, which are predicated on the assumption of Gaussianity. However, real-world datasets frequently violate this assumption, leading to biased and unreliable results. Moreover, these methodologies need improvement in effectively removing the influence of non-involved nodes on the COI, which would otherwise lead to misrepresenting causal relationships. On the other hand, conventional dimension reduction techniques in the time domain, such as principal component analysis (PCA), cannot fully capture the data's frequency-specific characteristics, which are crucial for understanding neural dynamics.

We propose a practical and easily accessible approach based on spectral dynamic principal component analysis (sDPCA) in the frequency domain, combined with permutation testing for Granger causality. The method sDPCA, initially proposed by Brillinger (1969, 1981), extends static PCA by incorporating temporal dependency within the data, thereby reducing the dimensionality of time series in the frequency domain while retaining maximal information. Various methodologies have evolved from sDPCA. For instance, Stoffer (1999) developed a spectral envelope using sDPCA to identify common signals across multiple time series, while Hörmann et al. (2015) proposed a functional variant of sDPCA for analyzing functional time-series data. Ombao and Ho. (2006), Yuxiao Wang et al. (2019), and Ombao and Pinto (2022) indicated that spectral principal component analysis (sPCA) in the frequency domain offers practical benefits and is highly effective in low-dimensional representations of high-dimensional time series. The main objective of this study is to illustrate how the proposed approach enables the practical and sufficient isolation of COI by partialling out the influence of disinterested nodes, which are derived as a dynamic summary in a low-dimensional representation. The frequency-domain dynamic PCA method maintains the spectral characteristics of the data, which are crucial for accurately determining causal relationships in time series networks. By employing a permutation-based GC test in lieu of the conventional F-test, we can relax with the assumption of normality in the error terms, thereby assuring robustness to deviations from normality and rendering the proposed approach more suitable for real-world data.

The proposed approach offers two main advantages. Firstly, DPCA in the frequency domain offers an accurate and practical dimension reduction while preserving the spectral information. This is also essential because EEGs are correlated across time, and hence, the spectrum captures cross-covariances at all lags. This leads to a more precise isolation of COI, reducing the likelihood of spurious causal inferences. Secondly, the permutation-based GC test improves the reliability of causality detection by not relying on the assumption of Gaussianity. This allows the test to accommodate distributions that deviate significantly from normality, such as the fat-tailed distributions observed often in EEG data. The procedure is straightforward and practical to apply. The subsequent sections will elaborate on the proposed approach and its components. Section 2 introduces the Spectral DPCA method and the permutation GC test. Section 3 outlines the scope of the simulation study and presents related results. Section 4 applies our approach to real EEG data and discusses the findings.

## 2 Methodology

### 2.1 Inference in high-dimensional networks of time series

Define  $N = \{Y_t^*, X_t^*, Z_{1,t}, \dots, Z_{n-2,t}\}$  to be a high dimensional network of time series with possibly  $n \geq 256$  nodes. As we consider in this paper, this network may represent the activity of a brain through EEG recordings in which each component (i.e., node or channel) is actually a time series. In this notation of network  $N$ ,  $Y^*$  and  $X^*$  denote any two nodes of interest. For problems whose solutions are sought in component-wise, we set our goal as exploring the interaction or efficient connectivity between any pair of nodes in a network rather than the relationality of the whole network. These two nodes are subject to the influence of other nodes due to the network's relational structure. This means that to dissect the respective efficient connection between any two nodes of interest, they need to be freed from the influences of other nodes. Thereby, the interference-free counterparts of the nodes of interest can be obtained in the following manner:

$$\begin{aligned} Y_t &= Y_t^* - E(Y_t^* | f_z(Z_{1,t}, \dots, Z_{n-2,t})), \\ X_t &= X_t^* - E(X_t^* | f_z(Z_{1,t}, \dots, Z_{n-2,t})), \end{aligned}$$

where the  $f_z(\cdot)$  is a function that ensures the dynamic variability of excluded nodes. Practically, the function  $f_z(\cdot)$  acts as a filter and can take any form as long as it provides the net summary discharge of the nodes excluded. Within the scope of this study, we utilize the spectral domain dynamic PCA implementation made available by Hörmann et al. (2015) via R package called `freqdom`. This method, originally proposed by Brillinger (1981), enables us to obtain principal component scores that concisely encapsulate variability in multi-dimensional time series, specifically with regard to their serial dependence (see, e.g., Shumway and Stoffer (2017), Ombao and Pinto (2022)). Hence, we propose the filter  $f_z(\cdot)$  over excluded nodes to provide the following summary indicators,

$$f_z(Z_{1,t}, \dots, Z_{n-2,t}) = \{pc1, pc2, \dots, pc_k, \text{interactions}\},$$

where  $pc_1, pc_2, \dots, pc_k$  are the scores of the principal components, and interactions represent any interaction terms between these principal components.

The conditional means with respect to these indicators are then given by:

$$E(Y_t^* | f_z(Z_{1,t}, \dots, Z_{n-2,t})) = a_1 \cdot pc_1 + a_2 \cdot pc_2 + \dots + a_k \cdot pc_k + \sum a_{ij} \cdot (pc_i \times pc_j),$$

$$E(X_t^* | f_z(Z_{1,t}, \dots, Z_{n-2,t})) = b_1 \cdot pc_1 + b_2 \cdot pc_2 + \dots + b_k \cdot pc_k + \sum b_{ij} \cdot (pc_i \times pc_j),$$

where  $pc_i$  represents the score of the  $i$ -th dynamic principal component and  $a_i, b_i, a_{ij}, b_{ij}$  are coefficients corresponding to the principal components and their interactions. The number of principal components  $k$  can be chosen to be relatively low compared to the number of dimensions, provided that they capture a sufficient proportion of the total variability in the network. For practical implementation, the first few principal components are generally sufficient.

**Spectral DPCA** The frequency domain dynamic PCA decomposes a multivariate time series into uncorrelated components in the frequency domain, maximizing the long-run variance explained. Unlike classical PCA, which produces components uncorrelated in space, sDPCA focuses on the spectral density of the data, producing components uncorrelated in time.

Assume a multivariate time series  $\mathbf{Z}$  of dimension  $T \times n$ , where  $T$  is the number of time points, and  $n$  is the number of variables; this can be considered as a network of time series. The first step in sDPCA involves estimating the spectral density matrix  $F(\omega)$  from the time series. The cross-spectral density for  $\mathbf{Z}$  can be defined as:

$$F_{\mathbf{Z}}(\omega) = \sum_{h \in \mathbb{Z}} \text{Cov}(\mathbf{Z}_h, \mathbf{Z}_0) \exp(-2\pi i h \omega),$$

where  $\text{Cov}(\mathbf{Z}_h, \mathbf{Z}_0)$  is the auto-covariance matrix at lag  $h$ . The empirical cross-spectral density can be estimated using a windowed version of the lagged auto-covariance matrices:

$$\hat{F}_{\mathbf{Z}}(\omega) = \sum_{|h| \leq q} w\left(\frac{|h|}{q}\right) \hat{C}_{\mathbf{Z}}(h) \exp(-2\pi i h \omega),$$

where  $w(\cdot)$  is a window function (i.e., kernel),  $q$  is the window size, and  $\hat{C}_{\mathbf{Z}}(h)$  is the empirical lagged auto-covariance given by:

$$\hat{C}_{\mathbf{Z}}(h) = \frac{1}{T} \sum_{t=1}^{T-|h|} (\mathbf{Z}_{t+|h|} - \bar{\mathbf{Z}})(\mathbf{Z}_t - \bar{\mathbf{Z}})',$$

for  $h \geq 0$ , and

$$\hat{C}_{\mathbf{Z}}(h) = \frac{1}{T} \sum_{t=|h|+1}^T (\mathbf{Z}_{t+|h|} - \bar{\mathbf{Z}})(\mathbf{Z}_t - \bar{\mathbf{Z}})',$$

for  $h < 0$ .

Once the spectral density matrix  $F(\omega)$  is obtained, the dynamic principal component filters  $\phi_k^{(j)}$  are computed, where  $k \in [-q, q] \subset \mathbb{Z}$  and the index  $j$  is referring to the  $j$ -th largest dynamic eigenvalue. The filters are derived as the Fourier coefficients of the dynamic eigenvectors  $\varphi_j(\omega)$  of the spectral density matrix  $F(\omega)$ :

$$\phi_k^{(j)} = \frac{1}{2\pi} \int_{-\pi}^{\pi} \varphi_j(\omega) \exp(-2ik\omega) d\omega.$$

The dynamic principal component scores  $dpc_t^{(j)}$  are then calculated by filtering the time series  $\mathbf{Z}_t$  with the dynamic principal component filters:

$$dpc_t^{(j)} = \sum_{k=-q}^q \phi_k^{(j)} \mathbf{Z}_{t-k}.$$

This convolution operation can be represented in matrix notation as:

$$\mathbf{dpc} = \mathbf{Z} * \Phi,$$

where  $*$  denotes the convolution operation.

The proportion of variance explained by the  $j$ -th dynamic principal component is quantified as:

$$v_j = \frac{\int_{-\pi}^{\pi} \lambda_j(\omega) d\omega}{\int_{-\pi}^{\pi} \text{tr}(F(\omega)) d\omega},$$

where  $\lambda_j(\omega)$  is the  $j$ -th dynamic eigenvalue of the spectral density matrix  $F(\omega)$ . This ratio provides a measure of how much of the total variance in the time series is captured by each dynamic principal component.

In summary, the sDPCA method involves estimating the spectral density matrix from the time series data using windowed empirical lagged auto-covariances and Fourier transform, computing dynamic principal component filters by performing eigendecomposition on the spectral density matrix and applying the inverse Fourier transform to the dynamic eigenvectors, obtaining dynamic principal component scores by filtering the time series with the computed filters, and quantifying the proportion of variance explained by each dynamic principal component. These steps collectively facilitate the decomposition of multivariate time series into components that are uncorrelated in time and maximize the long-run variance explained.

## 2.2 Permutation-based Granger Causality test

Granger Causality (GC) is a statistical hypothesis test used to determine whether one time series can predict another. The concept, introduced by Granger (1969), is based on the principle that if the prediction of a time series  $Y_t$  can be improved by incorporating past values of another time series  $X_t$ , then  $X_t$  is said to "Granger-cause"  $Y_t$ .

The Granger causality test involves the following steps. First, consider two time series  $X_t$  and  $Y_t$ . To test if  $X_t$  Granger-causes  $Y_t$ , we compare the following two models:

- Unrestricted Model:

$$Y_t = \alpha_0 + \sum_{i=1}^p \alpha_i Y_{t-i} + \sum_{j=1}^q \beta_j X_{t-j} + \epsilon_t$$

- Restricted Model:

$$Y_t = \gamma_0 + \sum_{i=1}^p \gamma_i Y_{t-i} + \eta_t$$

Here,  $p$  and  $q$  are the maximum lags considered,  $\alpha_0$  and  $\gamma_0$  are constants,  $\alpha_i$  and  $\gamma_i$  are coefficients of the lagged  $Y_t$ ,  $\beta_j$  are coefficients of the lagged  $X_t$ , and  $\epsilon_t$  and  $\eta_t$  are error terms.

To determine if  $X_t$  Granger-causes  $Y_t$ , we test the null hypothesis:

$$H_0 : \beta_1 = \beta_2 = \dots = \beta_q = 0$$

against the alternative hypothesis:

$$H_1 : \text{At least one } \beta_j \neq 0 \text{ for } j = 1, 2, \dots, q$$

The test statistic is based on the F-distribution and is computed as:

$$F = \frac{(RSS_R - RSS_U)/q}{RSS_U/(T - p - q - 1)},$$

where  $RSS_R$  and  $RSS_U$  are the residual sum of squares of the restricted and unrestricted models, respectively, and  $T$  is the number of observations. If the computed F-statistic is greater than the critical value from the F-distribution, we reject the null hypothesis, concluding that  $X_t$  Granger-causes  $Y_t$ .

Granger causality is widely used in fields such as economics, neuroscience, and environmental sciences. In neuroscience, it helps to understand the directional interactions between brain regions by analyzing EEG or fMRI data. However, conventional GC assumes that error terms are normally distributed and homoscedastic, which is often violated in practice, especially in EEG time series that exhibit heteroscedasticity and fat-tailed distributions. These violations can bias results.

Unobserved confounders can also complicate GC analysis. If external variables influencing both time series are omitted, the test might falsely identify causal relationships. This issue is particularly acute in complex systems with many interacting variables.

Permutation-based Granger causality (GC) testing offers a robust alternative to conventional GC tests by relaxing the Gaussianity assumption. The permutation-based GC test evaluates the significance of causality by comparing the observed test statistic against a distribution of test statistics generated through random permutations of the data. This approach is more robust to deviations from normality and other potential violations of the assumptions underlying conventional GC.

To perform the permutation test, we first calculate the test statistic,  $F$ , for the observed data. We then generate a distribution of the test statistic under the null hypothesis by randomly permuting the time series  $X_t$  and recomputing the F-statistic for each permutation. Specifically, we shuffle  $X_t$  to break any potential temporal structure and repeat the GC test for each permuted dataset. This creates a distribution of F-statistics that represent the null distribution.

The permutation p-value is then computed as the proportion of permuted test statistics that are greater than or equal to the observed test statistic:

$$p_{\text{perm}} = \frac{\sum_{k=1}^N \mathbf{1}(F_k \geq F_{\text{obs}})}{N}$$

where  $N$  is the number of permutations,  $F_k$  is the test statistic for the  $k$ -th permutation,  $F_{\text{obs}}$  is the observed test statistic, and  $\mathbf{1}(\cdot)$  is the indicator function. The indicator function  $\mathbf{1}(F_k \geq F_{\text{obs}})$  takes the value 1 if  $F_k$  is greater than or equal to  $F_{\text{obs}}$  and 0 otherwise. This function effectively counts the number of times the permuted test statistic exceeds the observed test statistic, providing a measure of how extreme the observed value is within the context of the null distribution.

This permutation approach provides a non-parametric method to assess the significance of the causality, making it more flexible and robust compared to traditional methods. By comparing the observed F-statistic to the distribution generated from permuted data, we account for the actual data distribution and potential dependencies, leading to more reliable inference.

### 3 Simulation study

The aim of the simulation study is to evaluate the effectiveness of spectral dynamic principal component analysis (sDPCA) combined with Granger causality (GC) testing in identifying true causal relationships within a high-dimensional network of time series data, specifically focusing on EEG data. The study investigates how well the proposed method isolates the channels of interest (COI) from the influences of other channels and accurately assesses their causal interactions.

The study begins by generating a set of 10 channels as mixtures of latent processes proposed by Ombao and Pinto (2022). Each latent process is modeled as an autoregressive process of order 2 (AR(2)). Mathematically, the channels and corresponding indexes are represented as:

$$Z_i(t) = a_i \cdot \delta(t) + b_i \cdot \theta(t) + c_i \cdot \alpha(t) + d_i \cdot \beta(t) + e_i \cdot \gamma(t) + \epsilon_i(t)$$

for  $i = 1, \dots, 5, 11, \dots, 15$ , where  $\delta, \theta, \alpha, \beta, \gamma$  are latent AR(2) processes, and  $\epsilon_i(t)$  are error terms.

Next, we generate another set of 10 channels, where each channel is caused by a corresponding channel from the first set with added noise. This can be represented as:

$$Z_{i+5}(t) = \phi_1 Z_i(t-1) + \phi_2 Z_i(t-2) + \phi_3 Z_i(t-3) + \phi_4 Z_i(t-4) + \epsilon_{i+5}(t)$$

for  $i = 1, \dots, 5, 11, \dots, 15$ . The error terms  $\epsilon_{i+5}(t)$  follow a specified distribution (e.g., t-distribution with degrees of freedom 15, normal distribution, or non-normal distribution with specified skewness and kurtosis).

The ground truth for Granger causality in this setup is defined by the following relationships:

$$Z_1 \rightarrow Z_6, \quad Z_2 \rightarrow Z_7, \quad Z_3 \rightarrow Z_8, \quad Z_4 \rightarrow Z_9, \quad Z_5 \rightarrow Z_{10}, \quad Z_{11} \rightarrow Z_{16}, \quad Z_{12} \rightarrow Z_{17}, \quad Z_{13} \rightarrow Z_{18}, \quad Z_{14} \rightarrow Z_{19}, \quad Z_{15} \rightarrow Z_{20}$$

The network is then extended by generating an additional 236 channels ( $Z_{21}$  to  $Z_{256}$ ) that share common latent processes with the first 20 channels. This ensures connectivity within the network. Some of these new channels are allowed to have linear influences on the first 20 channels and can be defined as:

$$Z_i(t) = Z_i(t) + \sum_{j \in \text{influencing set}} \text{weight} \cdot Z_j(t)$$

The number of influencing channels and the weight of their influence are varied in different scenarios to study their effect on the performance of the GC tests.

The study then applies sDPCA to the extended network, focusing on the 236 additional channels to isolate the COI (the first 20 channels). The principal component scores are used to remove the effects of the other channels on the COI. The adjusted time series are obtained by regressing the COI on the principal component scores and retaining the residuals. Bivariate component-wise VAR(1) models are fitted to the residuals to compute the F-statistics for the GC tests. These F-statistics are then compared to critical values from the F-distribution to decide on the presence of GC.

Finally, permutation-based F-statistics are computed by repeatedly permuting the predictor time series and recalculating the F-statistics. The proportion of permuted F-statistics that exceed the observed F-statistic provides the permutation p-value, offering a robust measure of causality that accounts for the actual data distribution.

The results are sensitive to the choice of latent processes and the influence of other channels. Different scenarios are explored by varying the number of influencing channels and the weight of their influence, with the goal of assessing the robustness and reliability of the proposed method in detecting true causal relationships within high-dimensional time series networks. For example, Table 1 presents the accuracy results for one of the simulation studies for different numbers of influencing nodes and varying weights on the COI in a high-dimensional network. The COI consists of the first 20 nodes out of a total of 256 nodes.

This simulation evaluates the performance of the sDPCA method with non-normal error terms, adding complexity due to potential spurious causal relationships. The study employs permutation-based Granger causality testing, detailed in Section 2, to robustly evaluate causal relationships without assuming normally distributed errors.

With 10 influencing nodes, sDPCA shows high accuracy, especially at lower weights (0.1), achieving 0.90 accuracy with 3 Ndpc. However, accuracy declines with higher weights (0.5 and 0.7), dropping to 0.60 and 0.35, respectively, indicating challenges in isolating true causal associations under heavier influences.

As the number of influencing nodes increases to 30, a similar pattern emerges. High accuracy persists at lower weights (0.1), but significantly decreases with higher weights, dropping to 0.30 at a weight of 0.7, underscoring the difficulty in maintaining accuracy with greater external influence.

With 60 and 90 influencing nodes, the challenge is more pronounced. For instance, with 60 influencing nodes and a weight of 0.7, accuracy falls to 0.20, highlighting the significant impact of increased external influences on the COI, complicating the isolation and accurate determination of true causal relationships.

Overall, this table shows that while the sDPCA method can effectively isolate the COI and maintain high accuracy in the presence of external influences, its performance is sensitive to the weight of the influence and the number of influencing nodes. Lower weights and fewer influencing nodes generally

Influencing Nodes = 10				
Ndpc	wt. = 0.1	wt. = 0.3	wt. = 0.5	wt. = 0.7
3	0.90	0.85	0.60	0.35
6	1.00	0.90	0.65	0.40
12	0.85	0.85	0.60	0.45
24	0.85	0.75	0.70	0.25
Influencing Nodes = 30				
Ndpc	wt. = 0.1	wt. = 0.3	wt. = 0.5	wt. = 0.7
3	0.90	0.35	0.15	0.30
6	0.85	0.80	0.30	0.25
12	1.00	0.85	0.40	0.40
24	0.95	0.60	0.35	0.20
Influencing Nodes = 60				
Ndpc	wt. = 0.1	wt. = 0.3	wt. = 0.5	wt. = 0.7
3	0.80	0.55	0.25	0.20
6	0.70	0.35	0.20	0.20
12	0.95	0.45	0.20	0.45
24	0.90	0.10	0.30	0.20
Influencing Nodes = 90				
Ndpc	wt. = 0.1	wt. = 0.3	wt. = 0.5	wt. = 0.7
3	0.90	0.30	0.20	0.15
6	0.85	0.15	0.30	0.20
12	0.80	0.25	0.30	0.30
24	0.85	0.40	0.35	0.25

Table 1: Accuracy results for varying numbers of influencing nodes and weights on the COI in a high-dimensional network under a different non-normal error mechanism with different skewness and kurtosis parameters,  $\epsilon \sim \text{non-Norm}(\mu = 0, \sigma = 1, \gamma = 0.5, \kappa = 0.5)$ . The COI consists of the first 20 nodes out of a total of 256 nodes. The numbers 10, 30, 60, 90 represent the number of nodes influencing the COI, and the values 0.1, 0.3, 0.5, 0.7 represent the weights of this influence.

result in higher accuracy, while higher weights and more influencing nodes pose greater challenges. These findings are consistent with the theoretical expectations discussed in our simulation framework, where the ability to isolate COI and accurately assess causal interactions is influenced by the degree of external interference. The use of permutation-based GC testing ensures that the assessment of causality is robust and not biased by the assumptions of normality, providing a more reliable analysis of the true causal relationships in the network.

Tables for additional simulations using different error mechanisms to generate the time series are provided in the appendix.

## 4 Application to EEG data

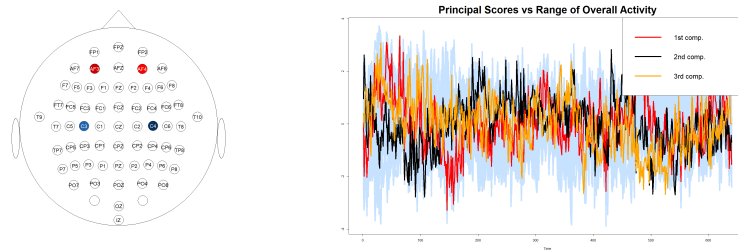
In this section, we demonstrate the utility of the proposed approach. For practical purposes, we focus on one epoch of the data and analyze four channels: AF3, AF4, C3, and C4. The dataset comes from an experiment involving a series of motor/imagery tasks, providing rich insights into the temporal dynamics of brain activity. The original EEG recordings were collected from 109 volunteers using the BCI2000 system with a 64-channel setup, and the data is publicly available at PhysioNet.org (Schalk et al., 2004). The experiment included 14 runs for each subject: two baseline runs (one with eyes open and one with eyes closed) and twelve task-oriented runs. During the task runs, participants either performed or imagined movements in response to visual cues, such as opening and closing fists or feet. The tasks were divided into categories: physical movement of the left or right

fist, imagined movement of the left or right fist, physical movement of both fists or both feet, and imagined movement of both fists or both feet.

Our main objective is to observe the effect of the sDPCA method on dimensionality reduction and its impact on the isolated channels. Specifically, we aim to determine whether this method distorts the temporal information in the time series. Consequently, we focus on only a few channels and share the results as an example, rather than conducting a detailed multichannel analysis. This allows us to provide a demonstration of the approach’s effectiveness in isolating channels of interest and assessing their causal interactions.

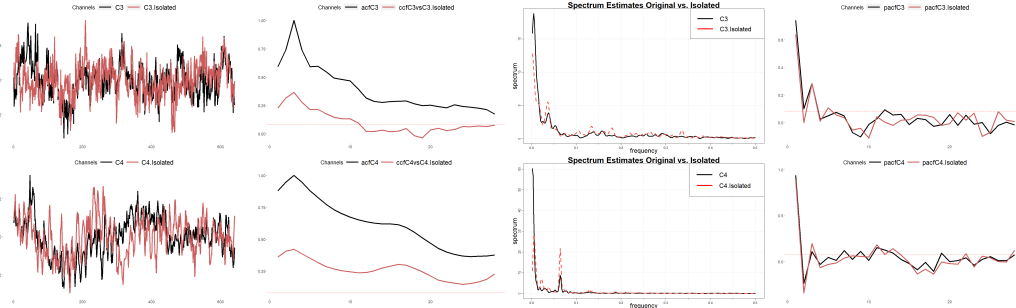
In Figure 1, the obtained three principal component (PC) scores are plotted over the time series data from which they were derived. This illustrates that the PC scores can capture the temporal structures of the high-dimensional time series from which they originate. This indicates that the obtained scores preserve the main characteristics of the time series, accurately representing their dynamics. This is a necessary finding that emphasizes the effectiveness and reliability of the procedure.

Figure 1: Isolating Nodes via Spectral Dynamic PCA method



Within the scope of this study, we compared the conditions before and after applying the spectral dynamic principal component analysis (sDPCA) method to the channels of interest. As illustrated in Figures 2 to 3, although the temporal characteristics of the series remain unchanged, there is a noticeable trend toward stationarity in the serial correlation amplitudes, which initially showed signs of non-stationarity. This adjustment indicates that while the sequential properties of the series are preserved, they become more aligned with the assumptions required by the auxiliary model used for Granger causality (GC) testing.

Figure 2: Sample vs Isolated channels C3 and C4.

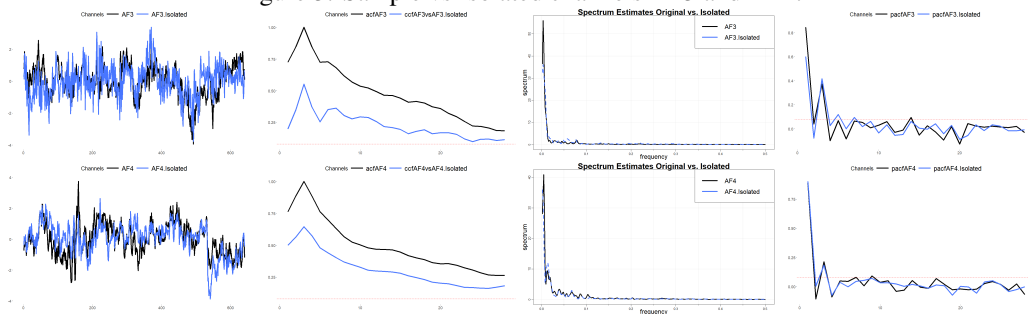


Moreover, our test results, summarized in Table 1, reveal significant differences in GC tests conducted before and after the isolation process. In several instances, the GC tests showed contrasting results after the isolation, underlining the presence of spurious GC causality in the original analysis. Specifically, we observed that causal relationships detected in the pre-isolation data were not present in the post-isolation data. This suggests that the influences of other channels, when not accounted for, can lead to misleading conclusions about causality.

Overall, these findings highlight the effectiveness of the sDPCA method in refining the data by removing extraneous influences, thereby providing a more accurate assessment of the true causal relationships within the EEG channels. This approach enhances the reliability of GC tests, ensuring that the detected causality is genuine and not a result of spurious interactions. The findings accentuate



Figure 3: Sample vs Isolated channels AF3 and AF4.



Direction of GC	GC result Before	GC result After
C3 → AF3	Cause	Do not cause
C3 → AF4	Cause	Cause
C4 → AF3	Do not cause	Do not cause
C4 → AF4	Cause	Cause
AF3 → C3	Cause	Do not cause
AF3 → C4	Cause	Cause
AF4 → C3	Cause	Cause
AF4 → C4	Do not cause	cause

Table 2: Comparison of Granger Causality Before and After Applying sDPCA

the capability of the sDPCA method to reduce the dimensionality of the data without losing temporal information.

## 5 Discussion and Conclusion

The study aims at improving the accuracy of Granger causal analysis in high-dimensional time-series networks, specifically focusing on EEG datasets. Through the use of the sDPCA method, we have been able to effectively isolate the COI from the influence of other channels within the network. The results of the simulation studies and the analysis of the real EEG signals show the simplicity, usefulness, and effectiveness of the proposed method.

The simulation study illustrates the challenges of identifying true causal interactions due to potential spurious causality, especially given the presence of non-normality. Integrating sDPCA and permutation-based GC testing significantly improved the accuracy of causal inference. The results show that the method maintained high accuracy in the presence of a moderate number of influencing nodes. However, the method’s accuracy decreases as the number of influencing nodes increases or approaches super/over connectivity (i.e., swarm-like neuronal connectivity). These findings underscore the sensitivity of GC to external influences and stress the necessity of accurately modeling such complexities in real-world data.

The application of the proposed approach to a network of EEG signals provided empirical validation of its potential utility. The principal component scores derived from the spectral domain accurately captured the temporal dynamics of the high-dimensional signals. The results indicate a convergence towards stationarity in the serial correlation amplitudes after applying sDPCA, getting the data closer to the assumptions demanded for reliable GC testing. The comparison of pre- and post-isolation GC results reveals the presence of spurious causality identification in the pre-isolation data, underlining the need to remove extraneous influences for accurate causality assessment.

Despite promising findings, there are several limitations to our study. Although comprehensive, the simulation framework may only capture some nuances of real EEG data. In addition, the test results can be significantly affected by the choice of hyper-parameters, such as the number of principal components, the weights, and the number of influencing nodes. These parameters need to be selected according to the specific characteristics of the datasets to be studied. Furthermore, our method’s reliance on linearity-based PCA in the frequency domain assumes that the underlying

temporal dynamics can be adequately captured, which may not always be the case. Future research should consider the integration of sDPCA with the perspective of capturing non-linear relationships. To further improve the robustness and accuracy of causal inference in complex networks, other dimensionality reduction techniques and advanced GC methods should be targeted. In addition, the applicability of the methodology could be significantly enhanced by extending it to include more sophisticated models of external influences and by incorporating real-time analysis capabilities.

In conclusion, our proposed approach provides a practical and reliable solution for isolating and analyzing causal associations in high-dimensional time series networks. The ability of the method to accurately identify true causal connections while mitigating the effects of confounding influences makes it a valuable tool for researchers in neuroscience and other fields dealing with complex time series data. The promising results of the study suggest that this approach can significantly improve the reliability of causality analysis, paving the way for more accurate and insightful investigations of the causal dynamics of high-dimensional networks.

## References

- Brillinger, D.R. (1969). The canonical analysis of stationary time series. *Multivariate analysis*, **2**, 331-350.
- Brillinger, D.R. (1981). *Time Series: Data Analysis and Theory*. Holden-Day, San Francisco, 540pp.
- Friston, K.J. (2011). Functional and effective connectivity: a review. *Brain connectivity*, **1**(1), 13-36.
- Friston, K., Moran, R., & Seth, A.K. (2013). Analyzing connectivity with Granger causality and dynamic causal modeling. *Current opinion in neurobiology*, **23**(2), 172-178.
- Hörmann, S., Kidziński, Ł., & Hallin, M. (2015). Dynamic functional principal components. *Journal of the Royal Statistical Society Series B: Statistical Methodology*, **77**(2), 319-348.
- Granger, C. W. (1969). Investigating causal relations by econometric models and cross-spectral methods. *Econometrica: journal of the Econometric Society*, 424-438.
- Schalk, G., McFarland, D.J., Hinterberger, T., Birbaumer, N., & Wolpaw, J. R. (2004). BCI2000: a general-purpose brain-computer interface (BCI) system. *IEEE Transactions on biomedical engineering*, **51**(6), 1034-1043.
- Shumway, R.H., & Stoffer, D.S. (2017). *Time series analysis and its applications* New York: Springer. <https://doi.org/10.1007/978-3-319-52452-8>
- Stoffer, D.S. (1999). Detecting common signals in multiple time series using the spectral envelope. *Journal of the American Statistical Association*, **94**(448), 1341-1356.
- Ombao, H., & Ho, M. H. R. (2006). Time-dependent frequency domain principal components analysis of multichannel non-stationary signals. *Computational statistics & data analysis*, **50**(9), 2339-2360.
- Ombao, H., & Pinto, M. (2022). Spectral dependence. *Econometrics and Statistics*. ISSN 2452-3062, <https://doi.org/10.1016/j.ecosta.2022.10.005>.
- Tu, T., Paisley, J., Haufe, S., & Sajda, P. (2019). A state-space model for inferring effective connectivity of latent neural dynamics from simultaneous EEG/fMRI. *Advances in Neural Information Processing Systems*, 32.
- Wang, Y., Ting, C. M., Gao, X., & Ombao, H. (2019, March). Exploratory analysis of brain signals through low dimensional embedding. *2019 9th International IEEE/EMBS Conference on Neural Engineering (NER)* (pp. 997-1002). IEEE.
- Yang, Y., Aminoff, E., Tarr, M., & Kass, R. E. (2016). A state-space model of cross-region dynamic connectivity in MEG/EEG. *Advances in neural information processing systems*, 29.

## A Appendix / supplemental material

Influencing Nodes = 10				
Ndpc	wt. = 0.1	wt. = 0.3	wt. = 0.5	wt. = 0.7
3	0.95	0.40	0.50	0.35
6	0.95	0.40	0.35	0.30
12	0.90	0.75	0.50	0.70
24	0.90	0.65	0.25	0.75
Influencing Nodes = 30				
Ndpc	wt. = 0.1	wt. = 0.3	wt. = 0.5	wt. = 0.7
3	0.90	0.40	0.40	0.25
6	0.90	0.40	0.25	0.40
12	0.80	0.50	0.45	0.45
24	0.80	0.35	0.45	0.40
Influencing Nodes = 60				
Ndpc	wt. = 0.1	wt. = 0.3	wt. = 0.5	wt. = 0.7
3	0.35	0.25	0.45	0.15
6	0.85	0.30	0.50	0.20
12	0.65	0.15	0.05	0.35
24	0.40	0.50	0.25	0.15
Influencing Nodes = 90				
Ndpc	wt. = 0.1	wt. = 0.3	wt. = 0.5	wt. = 0.7
3	0.80	0.35	0.30	0.45
6	0.55	0.30	0.25	0.15
12	0.40	0.40	0.20	0.30
24	0.30	0.30	0.20	0.20

Table 3: Accuracy results for varying numbers of influencing nodes and weights on the COI in a high-dimensional network under a non-normal error mechanism with different causal structure,  $\epsilon \sim \text{non-Norm}(\mu = 0, \sigma = 1, \gamma = 0.5, \kappa = 0.5)$ . The COI consists of the first 20 nodes out of a total of 256 nodes. The numbers 10, 30, 60, 90 represent the number of nodes influencing the COI, and the values 0.1, 0.3, 0.5, 0.7 represent the weights of this influence.

Influencing Nodes = 10				
Ndpc	wt. = 0.1	wt. = 0.3	wt. = 0.5	wt. = 0.7
3	0.95	0.75	0.75	0.45
6	0.85	0.75	0.45	0.05
12	0.95	0.75	0.75	0.60
24	1.00	0.90	0.60	0.50
Influencing Nodes = 30				
Ndpc	wt. = 0.1	wt. = 0.3	wt. = 0.5	wt. = 0.7
3	0.95	0.65	0.20	0.35
6	0.90	0.35	0.50	0.20
12	0.95	0.50	0.30	0.30
24	1.00	0.60	0.15	0.40
Influencing Nodes = 60				
Ndpc	wt. = 0.1	wt. = 0.3	wt. = 0.5	wt. = 0.7
3	0.90	0.20	0.25	0.20
6	0.85	0.50	0.20	0.40
12	0.85	0.40	0.25	0.30
24	0.90	0.15	0.15	0.35
Influencing Nodes = 90				
Ndpc	wt. = 0.1	wt. = 0.3	wt. = 0.5	wt. = 0.7
3	0.75	0.35	0.40	0.30
6	0.90	0.25	0.30	0.15
12	0.95	0.60	0.40	0.20
24	0.90	0.25	0.35	0.10

Table 4: Accuracy results for varying numbers of influencing nodes and weights on the COI in a high-dimensional network under non-normal error-generating mechanisms with different skewness and kurtosis parameters,  $\epsilon \sim \text{non-Norm}(\mu = -1, \sigma = 1, \gamma = 1.5, \kappa = 3.5)$ . The COI consists of the first 20 nodes out of a total of 256 nodes. The numbers 10, 30, 60, 90 represent the number of nodes influencing the COI, and the values 0.1, 0.3, 0.5, 0.7 represent the weights of this influence.

Influencing Nodes = 10				
Ndpc	wt. = 0.1	wt. = 0.3	wt. = 0.5	wt. = 0.7
3	0.95	0.90	0.60	0.45
6	0.90	0.90	0.50	0.45
12	0.90	0.90	0.50	0.20
24	1.00	0.95	0.70	0.55
Influencing Nodes = 30				
Ndpc	wt. = 0.1	wt. = 0.3	wt. = 0.5	wt. = 0.7
3	0.95	0.50	0.30	0.30
6	0.85	0.55	0.30	0.20
12	0.95	0.50	0.20	0.10
24	0.85	0.65	0.45	0.25
Influencing Nodes = 60				
Ndpc	wt. = 0.1	wt. = 0.3	wt. = 0.5	wt. = 0.7
3	0.85	0.35	0.05	0.20
6	0.75	0.30	0.25	0.35
12	0.90	0.35	0.15	0.30
24	0.80	0.55	0.45	0.25
Influencing Nodes = 90				
Ndpc	wt. = 0.1	wt. = 0.3	wt. = 0.5	wt. = 0.7
3	0.90	0.25	0.15	0.35
6	0.85	0.40	0.20	0.25
12	0.90	0.25	0.05	0.05
24	1.00	0.20	0.20	0.25

Table 5: Accuracy results for varying numbers of influencing nodes and weights on the COI in a high-dimensional network with Gaussian error-generating mechanisms. The COI consists of the first 20 nodes out of a total of 256 nodes. The numbers 10, 30, 60, 90 represent the number of nodes influencing the COI, and the values 0.1, 0.3, 0.5, 0.7 represent the weights of this influence.

Influencing Nodes = 10				
Ndpc	wt. = 0.1	wt. = 0.3	wt. = 0.5	wt. = 0.7
3	0.95	0.65	0.25	0.35
6	0.90	0.65	0.50	0.45
12	0.95	0.55	0.55	0.25
24	0.90	0.65	0.25	0.30
Influencing Nodes = 30				
Ndpc	wt. = 0.1	wt. = 0.3	wt. = 0.5	wt. = 0.7
3	0.90	0.55	0.20	0.10
6	0.70	0.65	0.30	0.30
12	0.75	0.55	0.50	0.35
24	0.75	0.65	0.40	0.30
Influencing Nodes = 60				
Ndpc	wt. = 0.1	wt. = 0.3	wt. = 0.5	wt. = 0.7
3	0.80	0.50	0.35	0.15
6	0.70	0.40	0.20	0.15
12	0.90	0.45	0.20	0.30
24	0.75	0.55	0.20	0.25
Influencing Nodes = 90				
Ndpc	wt. = 0.1	wt. = 0.3	wt. = 0.5	wt. = 0.7
3	0.55	0.25	0.35	0.30
6	0.55	0.60	0.15	0.25
12	0.65	0.20	0.30	0.25
24	0.45	0.30	0.15	0.20

Table 6: Accuracy results for varying numbers of influencing nodes and weights on the COI in a high-dimensional network with another Gaussian error-generating mechanism. The COI consists of the first 20 nodes out of a total of 256 nodes. The numbers 10, 30, 60, 90 represent the number of nodes influencing the COI, and the values 0.1, 0.3, 0.5, 0.7 represent the weights of this influence.

Influencing Nodes = 10				
Ndpc	wt. = 0.1	wt. = 0.3	wt. = 0.5	wt. = 0.7
3	1.00	0.60	0.70	0.30
6	0.90	0.40	0.40	0.35
12	0.95	0.15	0.25	0.30
24	1.00	0.40	0.45	0.70
Influencing Nodes = 30				
Ndpc	wt. = 0.1	wt. = 0.3	wt. = 0.5	wt. = 0.7
3	0.85	0.35	0.30	0.30
6	0.70	0.40	0.20	0.40
12	0.75	0.35	0.40	0.25
24	0.80	0.50	0.50	0.40
Influencing Nodes = 60				
Ndpc	wt. = 0.1	wt. = 0.3	wt. = 0.5	wt. = 0.7
3	0.40	0.50	0.35	0.15
6	0.50	0.70	0.30	0.25
12	0.50	0.40	0.25	0.25
24	0.40	0.60	0.20	0.40
Influencing Nodes = 90				
Ndpc	wt. = 0.1	wt. = 0.3	wt. = 0.5	wt. = 0.7
3	0.45	0.25	0.20	0.25
6	0.45	0.25	0.15	0.40
12	0.35	0.55	0.25	0.30
24	0.60	0.30	0.40	0.55

Table 7: Accuracy results for varying numbers of influencing nodes and weights on the COI in a high-dimensional network with another Gaussian error-generating mechanism. The COI consists of the first 20 nodes out of a total of 256 nodes. The numbers 10, 30, 60, 90 represent the number of nodes influencing the COI, and the values 0.1, 0.3, 0.5, 0.7 represent the weights of this influence.